

The influence of molecular shape and electronic properties on the formation of the ferroelectric nematic phase.

CRUICKSHANK, E., TUFAHA, N., WALKER, R., BROWN, S., GORECKA, E., POCIECHA, D., STOREY, J.M.D. and IMRIE, C.T.

2024

© 2024 The Author(s). Published by Informa UK Limited, trading as Taylor & Francis Group. This is an Open Access article distributed under the terms of the Creative Commons Attribution License (<http://creativecommons.org/licenses/by/4.0/>), which permits unrestricted use, distribution, and reproduction in any medium, provided the original work is properly cited.

The influence of molecular shape and electronic properties on the formation of the ferroelectric nematic phase

Ewan Cruickshank, Naila Tufaha, Rebecca Walker, Stevie Brown, Ewa Gorecka, Damian Pocięcha, John M.D. Storey & Corrie T. Imrie

To cite this article: Ewan Cruickshank, Naila Tufaha, Rebecca Walker, Stevie Brown, Ewa Gorecka, Damian Pocięcha, John M.D. Storey & Corrie T. Imrie (25 Jan 2024): The influence of molecular shape and electronic properties on the formation of the ferroelectric nematic phase, *Liquid Crystals*, DOI: [10.1080/02678292.2024.2304598](https://doi.org/10.1080/02678292.2024.2304598)

To link to this article: <https://doi.org/10.1080/02678292.2024.2304598>



© 2024 The Author(s). Published by Informa UK Limited, trading as Taylor & Francis Group.



[View supplementary material](#)



Published online: 25 Jan 2024.



[Submit your article to this journal](#)



[View related articles](#)



[View Crossmark data](#)

The influence of molecular shape and electronic properties on the formation of the ferroelectric nematic phase

Ewan Cruickshank ^{a*}, Naila Tufaha ^a, Rebecca Walker ^a, Stevie Brown ^a, Ewa Gorecka ^b, Damian Pociecha ^b, John M.D. Storey ^a and Corrie T. Imrie ^a

^aDepartment of Chemistry, University of Aberdeen, Old Aberdeen, UK; ^bFaculty of Chemistry, University of Warsaw, Warsaw, Poland

ABSTRACT

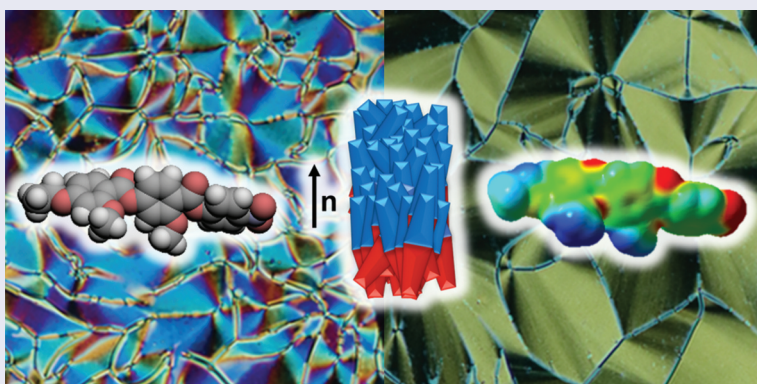
The synthesis and characterisation of two series of ferroelectric nematogens based on RM734 having an additional methoxy group on the central phenyl ring are reported, the 3-methoxy-4-((4-nitrophenoxy)carbonyl)phenyl 2-alkoxy-4-alkoxybenzoates (**7-*m-n***) and the 3-methoxy-4-((3-fluoro-4-nitrophenoxy)carbonyl)phenyl 2-alkoxy-4-alkoxybenzoates (**8-*m-n***). In order to compare the behaviour of these series to those of the corresponding materials that do not contain the methoxy group on the central phenyl ring, we also report the synthesis and characterisation of 4-[(4-nitrophenoxy)carbonyl]phenyl 4-methoxybenzoate (**11-0-1**), 4-[(3-fluoro-4-nitrophenoxy)carbonyl]phenyl 4-methoxybenzoate (**12-0-1**) and 4-[(3-fluoro-4-nitrophenoxy)carbonyl]phenyl 2,4-diethoxybenzoate (**12-2-2**). Two compounds in which a lateral ethoxy chain is attached to the central ring, 3-ethoxy-4-[(4-nitrophenoxy)carbonyl]phenyl 2,4-dimethoxybenzoate (**18-2-1**) and 3-ethoxy-4-[(3-fluoro-4-nitrophenoxy)carbonyl]phenyl 2,4-dimethoxybenzoate (**19-2-1**), are also described. The behaviour of these materials shows that the relative stabilities of the ferroelectric nematic, N_F , and conventional nematic, N , phases are governed by a subtle interplay of steric and electronic factors. Furthermore, the electronic factors are better understood in terms of isolated regions of electron density rather than by a single large longitudinal dipole moment. In terms of molecular shape, to observe the N_F phase it appears that the molecular structure must include one or more lateral substituents that enhance molecular biaxiality and destabilise the N phase.

ARTICLE HISTORY

Received 18 August 2023
Accepted 2 January 2024

KEYWORDS

Ferroelectric nematic phase; fluorine; lateral substituents; liquid crystals; nematic phase




Introduction

The conventional nematic phase, N , underpins the multi-billion dollar liquid crystal display, LCD, industry [1,2] and although in recent years alternative technologies such as OLED displays have acquired significant market share, LCDs have continued to develop and improve, including, for example, the introduction of quantum dot backlights [3,4]. This has ensured that

LCDs remain the prevalent display technology. It is the case, however, that LCDs are a mature technology, and it is imperative that novel phases exhibiting new electro-optic properties are discovered to underpin the next generation LCD. In this regard, the recent discovery of the ferroelectric nematic phase is highly relevant and topical, and has quickly become the hottest topic in the field [5,6].

CONTACT Ewan Cruickshank  e.cruickshank2@rgu.ac.uk

*School of Pharmacy and Life Sciences, Robert Gordon University, Aberdeen, AB10 7GJ, U.K.

 Supplemental data for this article can be accessed online at <https://doi.org/10.1080/02678292.2024.2304598>.

© 2024 The Author(s). Published by Informa UK Limited, trading as Taylor & Francis Group.

This is an Open Access article distributed under the terms of the Creative Commons Attribution License (<http://creativecommons.org/licenses/by/4.0/>), which permits unrestricted use, distribution, and reproduction in any medium, provided the original work is properly cited. The terms on which this article has been published allow the posting of the Accepted Manuscript in a repository by the author(s) or with their consent.

In the conventional N phase, the long axes of the rod-like molecules align more or less in a preferred direction known as the director, \mathbf{n} , but their centres of mass are randomly distributed as in an isotropic liquid. The director has inversion symmetry such that $\mathbf{n} = -\mathbf{n}$, [Figure 1](#), and the phase is non-polar. Over a century ago Born speculated that a polar fluid should exist if the dipoles of the constituent molecules were sufficiently large such that the dipole-dipole interactions between them could overcome thermal fluctuations [7]. Some 90 years later, computer simulations of tapered Gay-Berne particles with a longitudinal dipole moment revealed ferroelectric nematic, N_F , behaviour [8, 9]. The N_F phase remained experimentally elusive until 2017, when two groups independently reported materials that are now understood to exhibit polar nematic phases. The compounds in question are referred to as RM734 [10] and DIO [11] and were shown to exhibit the N_F phase [12] in which the director does not possess inversion symmetry, $\mathbf{n} \neq -\mathbf{n}$, and the phase is polar, [Figure 1](#). The N_F phase has huge application potential and underpinning this are properties including ease of alignment [13, 14], strong non-linear optical response [15–19], high polarisation values [11, 12, 20, 21], large dielectric permittivities [22–30], and switching at very low electric fields [11, 12, 24, 31–36].

In order for the huge application potential of the N_F phase to be realised, new ferroelectric nematogens are required having tailored properties and to achieve this requires a better understanding of the structure-property relationships for this class of materials. This endeavour will lead to the discovery of new phase behaviour such as the recently reported ferroelectric smectic A phase [34,37,38]. We have previously reported a range of ferroelectric nematogens based on RM734 in which the length of the lateral alkoxy chain was varied in addition to its position in the molecule [18,36,39,40]. In these materials, it was found that the

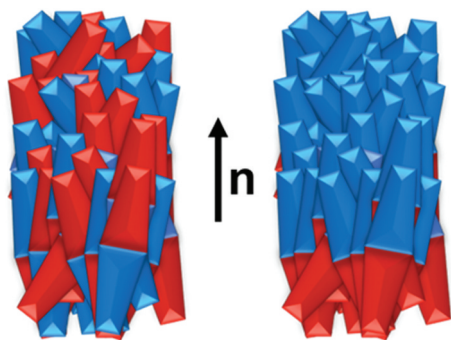


Figure 1. (Colour online) Schematic representations of the conventional nematic, N, phase (left) and the polar ferroelectric nematic, N_F , phase (right).

N_F phase was observed even for molecules with long lateral chains, although both the N and N_F phases were destabilised as the lateral chain length increased, as reported by Mandle *et al.* [10]. These compounds contained a single lateral substituent. Here, we extend this design approach and report compounds having two lateral alkoxy groups with the expectation that direct N_F -I transitions may be seen [18,23,25,28,29,36,40,41]. Specifically, we report the synthesis and characterisation of two series of ferroelectric nematogens based on RM734 but that have an additional methoxy group on the central phenyl ring, the 3-methoxy-4-((4-nitrophenoxy)carbonyl)phenyl 2-alkoxy-4-alkoxybenzoates (**7- m - n**) and the 3-methoxy-4-((3-fluoro-4-nitrophenoxy)carbonyl)phenyl 2-alkoxy-4-alkoxybenzoates (**8- m - n**), [Figure 2](#). In the acronyms used to refer to these compounds, m is the length of the lateral alkoxy chain and n is the length of the terminal alkoxy chain. The structural difference between these series is the addition of a fluorine atom *ortho* to the terminal nitro group in the **8- m - n** series, and this allows for the effects of molecular polarity and polarisability on the N_F phase to also be considered. In order to compare the behaviour of these series to those of the corresponding materials that do not contain the methoxy group on the central phenyl ring, we also report the synthesis and characterisation of 4-[(4-nitrophenoxy)carbonyl]phenyl 4-methoxybenzoate (**11-0-1**), 4-[(3-fluoro-4-nitrophenoxy)carbonyl]phenyl 4-methoxybenzoate (**12-0-1**) and 4-[(3-fluoro-4-nitrophenoxy)carbonyl]phenyl 2,4-diethoxybenzoate (**12-2-2**), members of the **11- m - n** and **12- m - n** series, [Figure 3](#). Finally, we also report two compounds in which a lateral ethoxy chain is attached to the central ring, namely, 3-ethoxy-4-[(4-nitrophenoxy)carbonyl]phenyl 2,4-dimethoxybenzoate (**18-2-1**) and 3-ethoxy-4-[(3-fluoro-4-nitrophenoxy)carbonyl]phenyl 2,4-dimethoxybenzoate (**19-2-1**), [Figure 4](#).

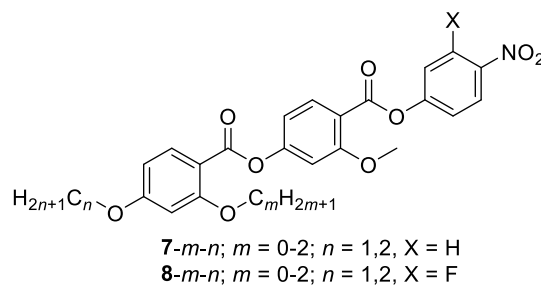


Figure 2. Molecular structures of the **7- m - n** and **8- m - n** series; m is the number of carbons in the lateral alkoxy chain and n is the number of carbons in the terminal alkoxy chain. For $m = 0$ the lateral group is a H atom.

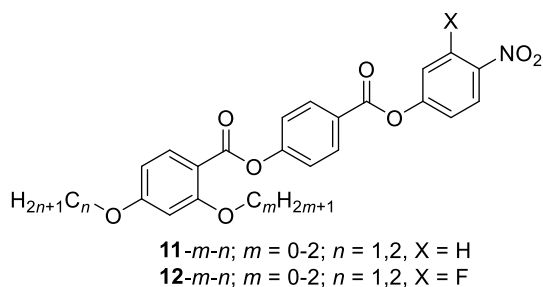


Figure 3. Molecular structures of the $11-m-n$ and $12-m-n$ series; m is the number of carbons in the lateral alkoxy chain and n is the number of carbons in the terminal alkoxy chain. For $m = 0$ the lateral group is a H atom.

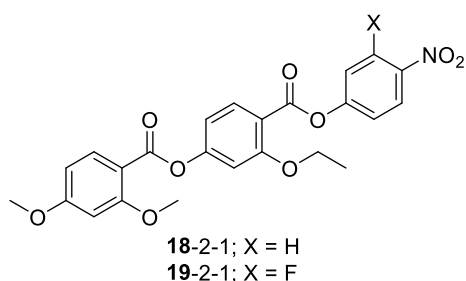


Figure 4. Molecular structures of $18-2-1$ and $19-2-1$.

Experimental

Synthesis

The synthetic routes used to prepare the $7-m-n$ and $8-m-n$ series are shown in Scheme 1, for $11-0-1$, $12-0-1$ and $12-2-2$ in Scheme 2, and for $18-2-1$ and $19-2-1$ in Scheme 3. These syntheses are based on methods which have been reported by Li *et al.* [22,23]. A detailed description of the preparation of both series, including the structural characterisation data for all intermediates and final products, is provided in the Supplementary Information.

Optical studies

Phase characterisation was performed by polarised light microscopy, using an Olympus BH2 polarising light microscope equipped with a Linkam TMS 92 hot stage or a Zeiss AxioImager A2m equipped with a Linkam THMS600 hot stage. The untreated glass slides were 0.17 mm thickness. The cells treated for planar alignment were purchased from INSTEC with a cell thickness between 2.9 and 3.5 μm or with homeotropic alignment from WAT with a cell thickness of 1.6 μm .

Differential scanning calorimetry

The phase behaviour of the materials was studied by differential scanning calorimetry performed using

Mettler Toledo DSC1 or DSC3 differential scanning calorimeters equipped with TSO 801RO sample robots and calibrated using indium and zinc standards. Heating and cooling rates were $10^\circ\text{C min}^{-1}$, with a 3-min isotherm between either heating or cooling, and all samples were measured under a nitrogen atmosphere. Transition temperatures and associated enthalpy changes were extracted from the heating traces unless otherwise noted. The entropy changes associated with the transitions observed were reported scaled by the universal gas constant, R , using a value of $8.314 \text{ J K}^{-1} \text{ mol}^{-1}$.

Molecular modelling

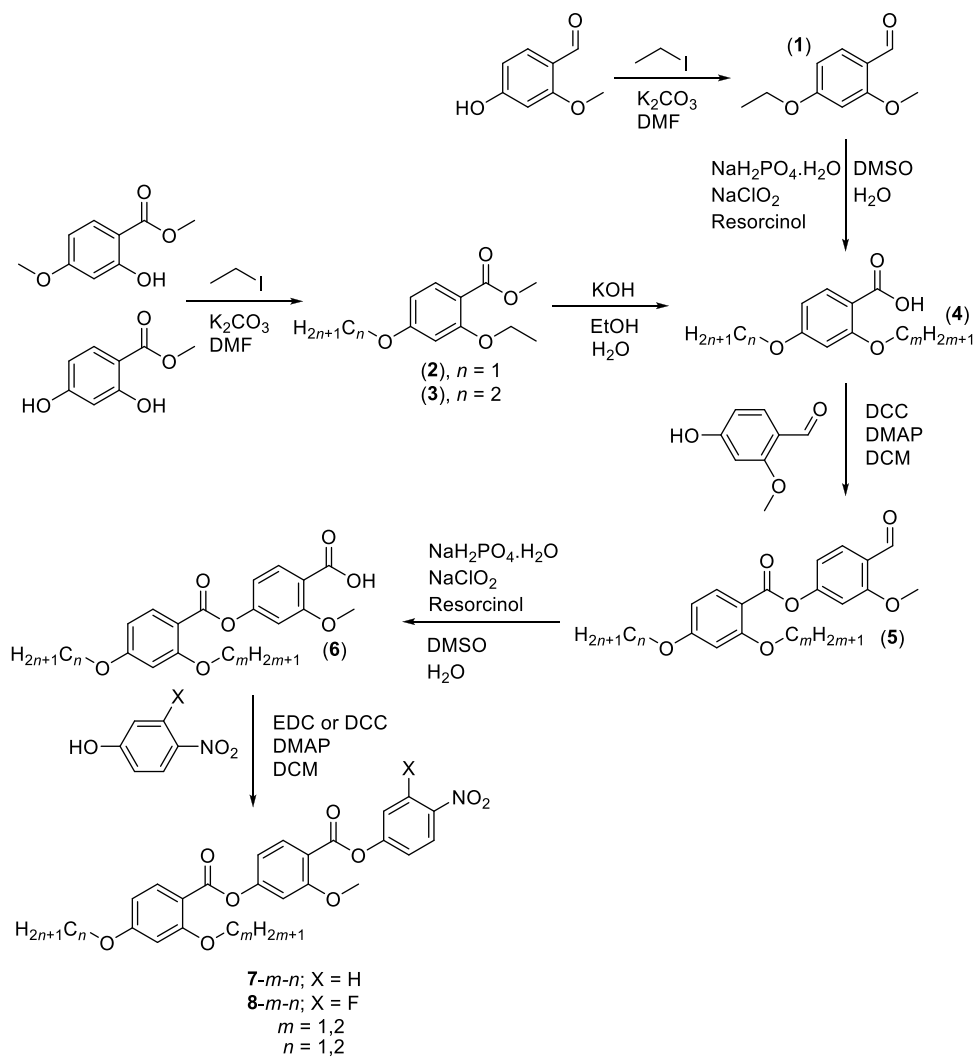
The geometric parameters of the compounds of interest were obtained using quantum mechanical DFT calculations with Gaussian09 software [42]. Optimisation of the molecular structures was carried out at the B3LYP/6-31G(d) level of theory. A frequency check was used to confirm that the minimum energy conformation found was an energetic minimum. The relative orientations of the ester groups were varied, and it was found that inverting either, such that they were no longer parallel, reduced the molecular dipole moment by $\approx 1.7 \text{ D}$, but that these conformations were unfavourable. Visualisations of electronic surfaces and ball-and-stick models were generated from the optimised geometries using the GaussView 5 software. The electronic surfaces were found with the cubegen utility in GaussView by generating a total density cube using a SCF density matrix and coarse grid, overlaid by an ESP surface map. Visualisations of the space-filling models were produced post-optimisation using the QuteMol package [43].

Spontaneous electric polarisation measurements

Spontaneous electric polarisation was determined by integration of the current peaks recorded during Ps switching upon applying a triangular voltage (22 Hz, 140 V_{pp}). The 5- μm -thick cell with ITO electrodes and no polymer aligning layers were used, and the switching current was determined by recording the voltage drop at the resistivity of 2 $\text{k}\Omega$ in serial connection with the sample. It was checked that under such conditions the saturated values of polarisation were obtained.

Dielectric spectroscopy

The complex dielectric permittivity, ϵ^* , was measured using a Solartron 1260 impedance analyser, in the 1 Hz



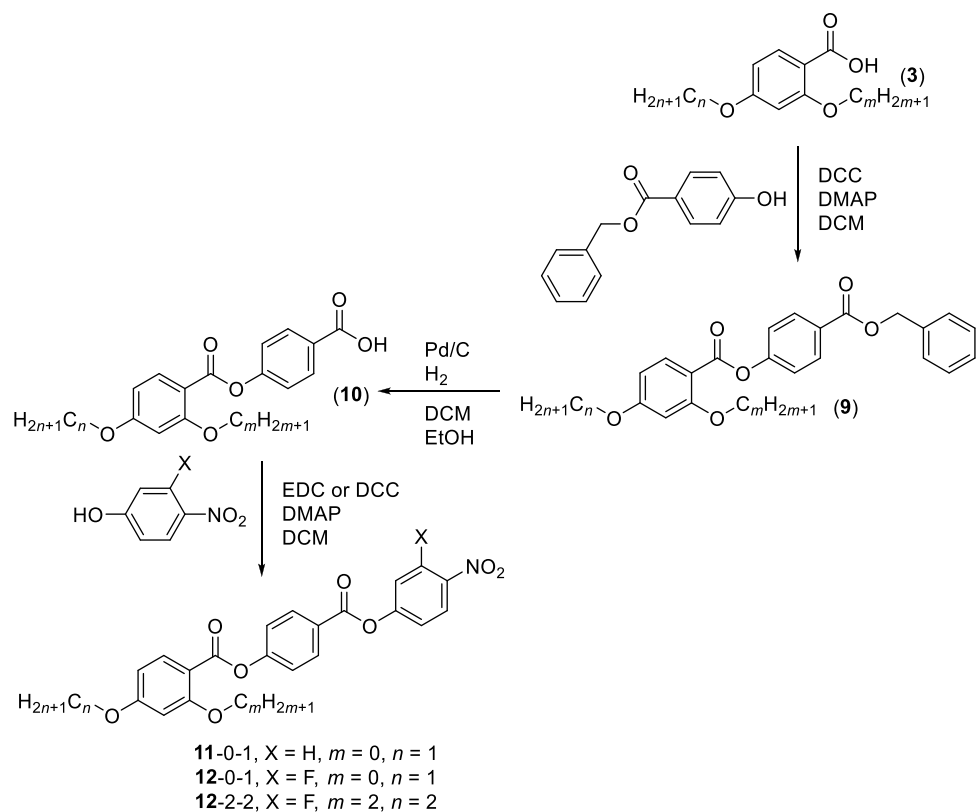
Scheme 1. Synthetic route for the $7-m-n$ and $8-m-n$ series.

–1 MHz frequency (f) range, with the probe voltage 20 mV. The material was placed in a 5- μm -thick glass cell with ITO electrodes. The electrodes were not covered with polymer aligning layers, as the presence of the thin (~ 10 nm) polyimide layers at the cell surfaces acts as an additional high capacitance being in a series circuit with the capacitor filled with the LC sample, and for the materials studied here with very high values of permittivity, this may strongly affect the measured permittivity of the LC phases. Lack of a surfactant layer resulted in a random configuration of the director in the LC phase.

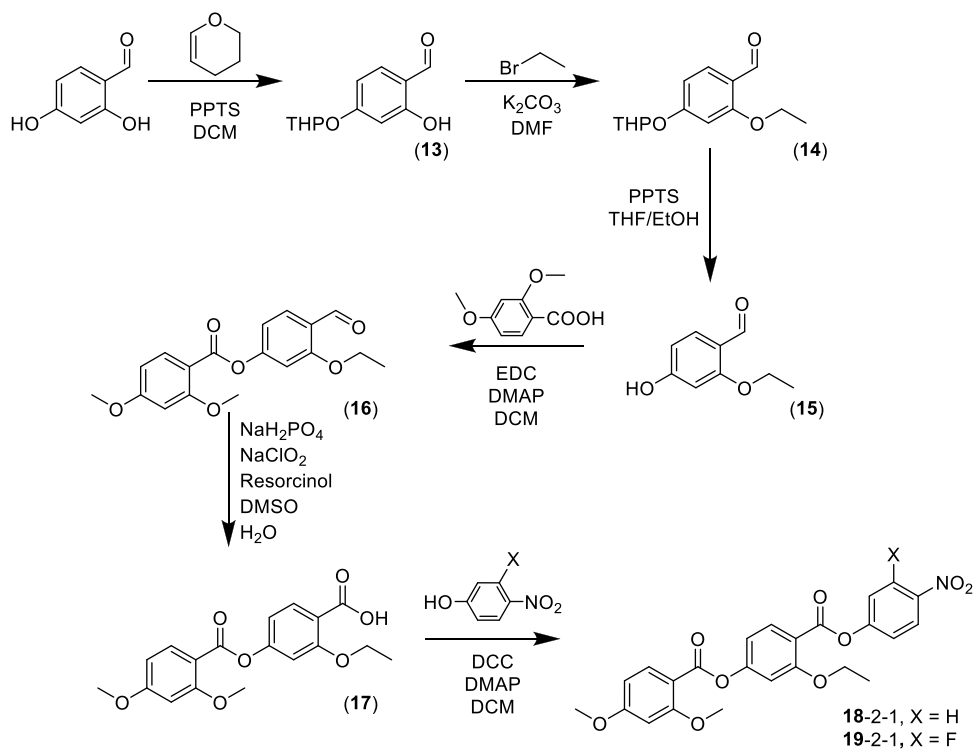
Results

The transitional properties of the $7-m-n$ series are reported in Table 1. For comparative purposes, the data for 7-0-1 extracted from the literature have also been included [36]. The transitional properties of 7-1-1 were in good agreement with those reported previously

[23]. All the new members of the $7-m-n$ series exhibited a ferroelectric nematic phase which formed directly from the isotropic liquid. The phase assignments were made using polarised optical microscopy with the transition to the N_F phase being marked by the emergence of highly birefringent circular droplets which grew on cooling as described elsewhere [22,28,36,40,44]. These droplets coalesced, Figure, and, in untreated glass slides, domains formed separated by domain boundaries, Figure 5(b). These domains are thought to be indicative of areas in which the director has differing orientations and thus the orientation of the polarisation also differs. In cells treated for planar alignment, the domain structure is more distinct, Figure 5(c). This texture has been described as ‘banded’ due to the differing areas of birefringence within the domains, and appears to be characteristic of the N_F phase particularly when viewed in cells treated for planar alignment [22,29,36,39,40]. The values of the scaled entropy change associated with the



Scheme 2. Synthetic route for **11-0-1**, **12-0-1** and **12-2-2**.



Scheme 3. Synthetic route for **18-2-1** and **19-2-1**.

Table 1. Transition temperatures and associated entropy changes for the **7-*m-n*** series. The calculated dipole moments, μ , are also listed. The data for **7-0-1** have been extracted from Tufaha *et al.* [36].

<i>m</i>	<i>n</i>	$T_{\text{CrI}}/^{\circ}\text{C}$	$T_{\text{N}_F}/^{\circ}\text{C}$	$T_{\text{N}_I}/^{\circ}\text{C}$	$\Delta S_{\text{CrI}}/R$	$\Delta S_{\text{N}_F}/R$	$\Delta S_{\text{N}_I}/R$	μ/D
0	1	192	^a 126	^a 189	12.5	^a 0.032	^a 0.21	11.59
1	1	167	^a 104	-	15.1	^a 1.34	-	12.73
1	2	134	^a 97	-	15.1	^a 1.23	-	13.06
2	1	145	^a 81	-	13.5	^a 1.13	-	12.58
2	2	130	^a 79	-	13.7	^a 0.82	-	12.90

^aValues extracted from DSC cooling traces.

N_F -I transition, $\Delta S_{\text{N}_F}/R$, listed in Table 1 are several times larger than $\Delta S_{\text{N}_I}/R$ for **7-0-1**, and similar to those reported elsewhere for the N_F -I transition [36,40]. This additional entropic contribution is thought to be associated with the ordering of the dipoles in the N_F phase.

The transitional properties of the **8-*m-n*** series are reported in Table 2 and also included are the corresponding data for **8-0-1** extracted from the literature [36]. As with the **7-*m-n*** series, all the members of the **8-*m-n*** series except **8-0-1** showed direct N_F -I transitions. The N_F phase in the **8-*m-n*** series was assigned based on the observation of similar textures to those described earlier, with representative textures obtained for samples viewed in cells treated for planar alignment as shown in Figure 6(a,b). For samples viewed between untreated glass slides the textures are not so

characteristic of the N_F phase, Figure 6(c), and more reminiscent of the schlieren texture seen for the conventional nematic phase. The values of the entropy change associated with the N_F -I transition are large, see Table 2, and similar to those reported for the **7-*m-n*** series. The N_F phase assignment was confirmed for compound **8-2-2** by measurements of spontaneous electric polarisation (Ps) and by dielectric spectroscopy, Figure 7. The measured value of the spontaneous electric polarisation was $6.4 \mu\text{C cm}^{-2}$ (10°C below the Iso- N_F phase transition), and this is typical for the ferroelectric nematic phase. The value of Ps was nearly temperature independent. The polar character of the N_F phase was manifested by the appearance of a strong dielectric relaxation mode [18,23–25,28,29,36], with

Table 2. Transition temperatures and associated entropy changes for the **8-*m-n*** series. The calculated dipole moments, μ , are also listed. The data for **8-0-1** have been extracted from Tufaha *et al.* [36].

<i>m</i>	<i>n</i>	$T_{\text{CrI}}/^{\circ}\text{C}$	$T_{\text{N}_F}/^{\circ}\text{C}$	$T_{\text{N}_I}/^{\circ}\text{C}$	$\Delta S_{\text{CrI}}/R$	$\Delta S_{\text{N}_F}/R$	$\Delta S_{\text{N}_I}/R$	μ/D
0	1	180	^a 142	^a 157	13.7	^a 0.34	^a 0.28	12.64
1	1	204	^a 99	-	15.8	^a 1.23	-	13.77
1	2	131	^a 86	-	10.9	^a 1.10	-	14.10
2	1	174	^a 82	-	15.7	^a 0.86	-	13.64
2	2	133	^a 76	-	15.6	^a 1.39	-	14.02

^aValues extracted from DSC cooling traces.

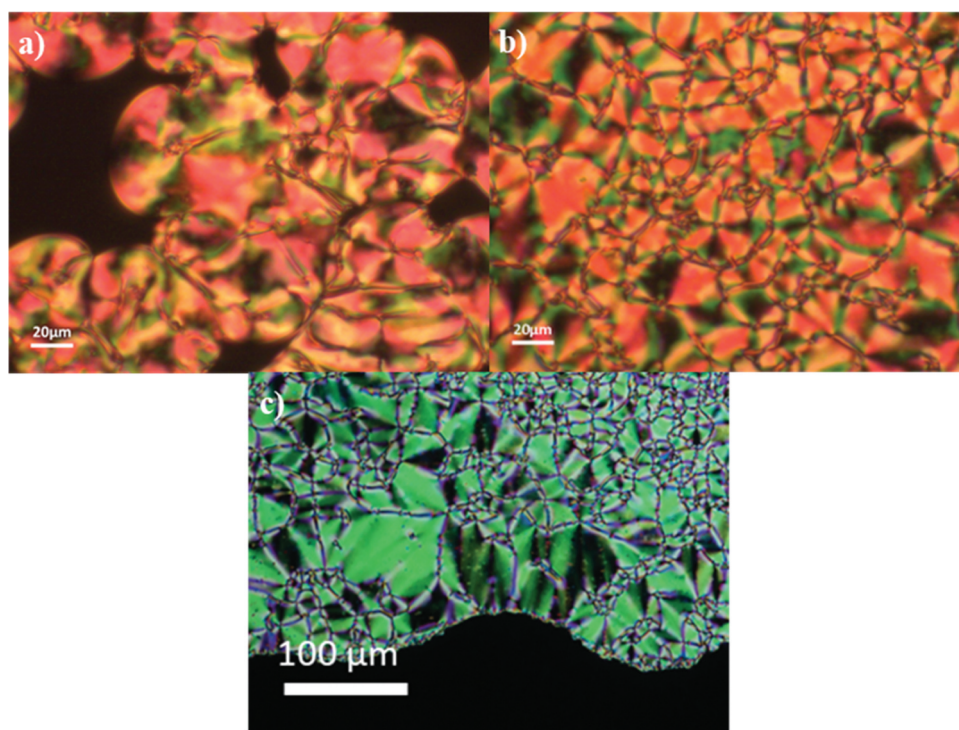


Figure 5. (Colour online) Polarised optical microscope textures observed for the **7-*m-n*** series: (a) coalescence of droplets at the N_F -I phase transition for **7-1-1** in untreated glass slides ($T = 104^{\circ}\text{C}$), (b) banded texture of the N_F phase in **7-2-1** in untreated glass slides ($T = 80^{\circ}\text{C}$), (c) banded texture of the N_F phase in **7-2-2** in a cell treated for planar alignment ($T = 70^{\circ}\text{C}$).

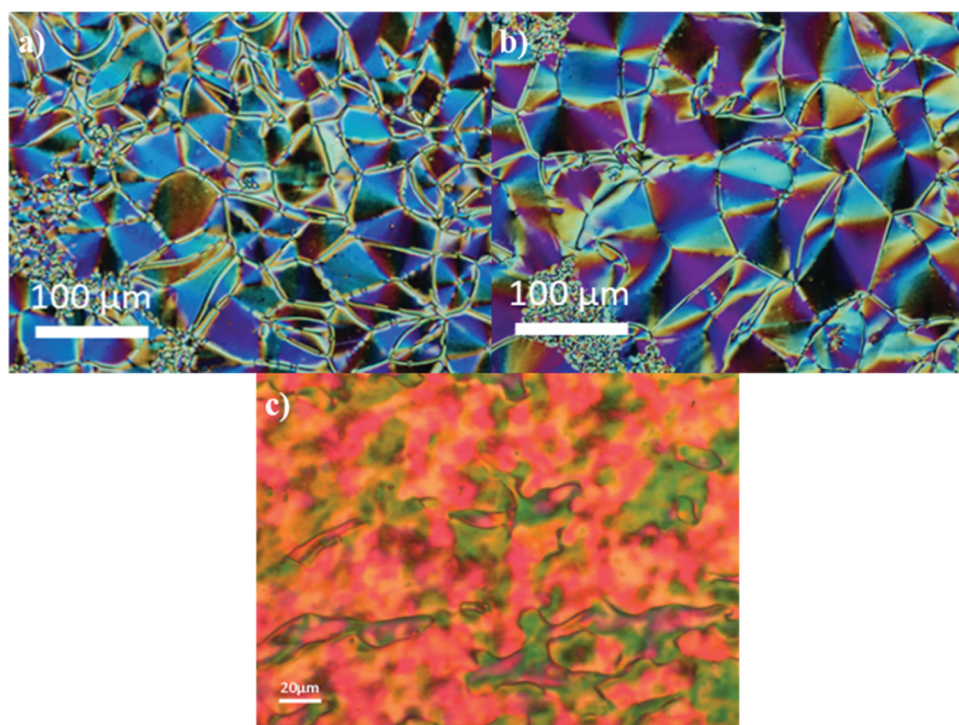


Figure 6. (Colour online) Polarised optical microscope textures observed for the **8-*m-n*** series: (a) banded texture of the N_F phase in **8-2-1** in a planar aligned cell ($T = 80^\circ\text{C}$), (b) banded texture of the N_F phase in **8-1-2** in a cell treated for planar alignment ($T = 80^\circ\text{C}$), (c) uncharacteristic texture of the N_F phase in **8-2-2** in a cell treated for planar alignment ($T = 75^\circ\text{C}$).

the relaxation frequency ≈ 500 Hz directly below the $I-N_F$ phase transition; the relaxation frequency decreased to a sub-Hz regime 40°C below the transition, due to the strongly increasing viscosity of the material. The dielectric strength, $\Delta\epsilon \approx 7000$, was almost temperature independent and this mode has been assigned to the collective movement of the polarisation vector direction, the phason mode [30].

The transitional properties of **18-2-1** and **19-2-1** are reported in Table 3, and both exhibit N_F-I transitions. The N_F phase was assigned again by the observation of a banded texture, with a representative example shown in Figure 8. The high values of $\Delta S_{N_F-I}/R$ are consistent with these phase assignments.

The transitional properties of the **11-*m-n*** and **12-*m-n*** series, see Figure 3, are listed in Table 4. We note that the extensively studied ferroelectric nematogen RM734 corresponds to **11-1-1** using our numbering system. For comparative purposes, we have also listed the transitional data for **11-1-2**, **11-2-2**, **12-1-1** and **12-1-2** extracted from the literature [10,45]. The data listed for **11-1-1**, **11-2-1** and **12-2-1** have been reported previously by ourselves [18,25,40]. The transition temperatures reported for **11-0-1** are in good agreement with those reported in literature albeit we report higher values [46]. **12-0-1** showed only the conventional nematic phase assigned by the observation of

a characteristic schlieren texture. **12-2-2** exhibited both the ferroelectric and conventional nematic phases. On cooling the isotropic phase, a characteristic schlieren texture containing two- and four-brush point defects formed in untreated glass slides and a uniform planar texture if viewed in a cell treated for planar alignment, Figure 9(a). In addition, the sample flashed when subjected to mechanical stress. The ferroelectric nematic phase was assigned by the observation of textures described earlier, and a representative example is given in Figure 9(b).

Discussion

We now turn our attention to how the changes in molecular structure affect the liquid crystalline behaviour in this group of materials. Compound **11-0-1** contains no lateral methoxy groups and only shows a conventional N phase with an associated T_{NI} of 284°C . The addition of a methoxy group in a *meta* position to the terminal methoxy group gives **11-1-1** (RM734) and T_{NI} falls by 96°C with an N_F-N transition now seen at 131°C . If instead, the methoxy group is added to the central ring giving **7-0-1**, then T_{NI} falls by essentially the same amount, 95°C , but T_{N_F-N} is a little lower, 126°C . The addition of both methoxy groups to the structure of **11-0-1** to give **7-1-1** sees a decrease in

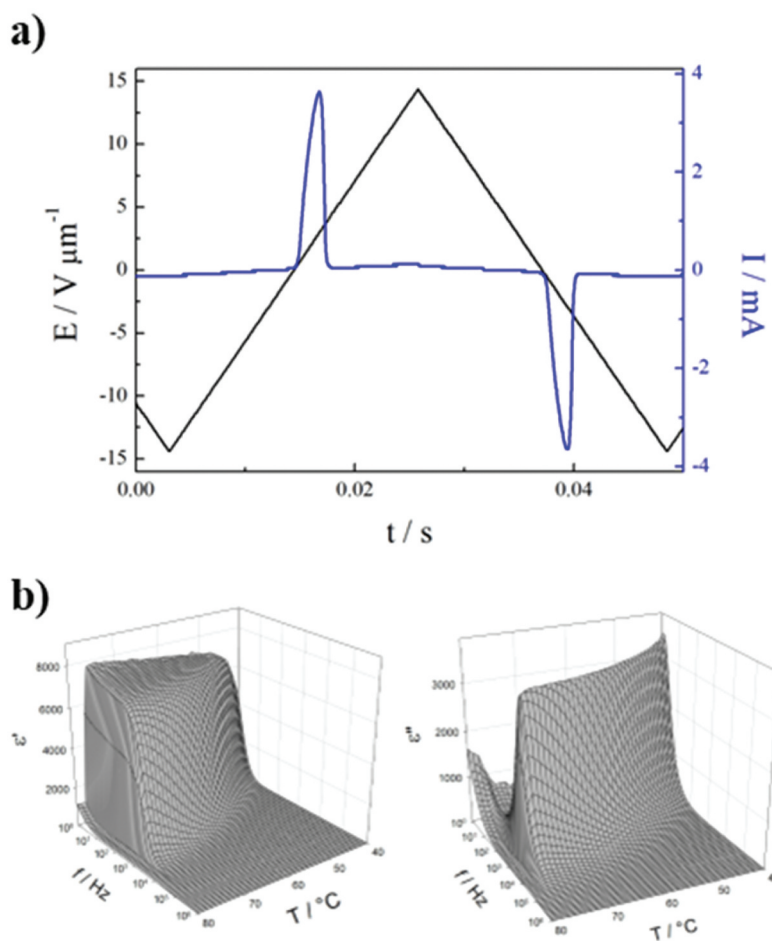


Figure 7. (Colour online) (a) The switching current (blue line) associated with polarisation reversal under an applied triangular wave voltage (black line) for **8-2-2** at 65°C. Measurements were performed in a 5- μm -thick cell with ITO electrodes and no alignment layer. (b) Real (left) and imaginary (right) parts of the complex dielectric permittivity measured vs temperature and frequency for **8-2-2**, in a 5- μm -thick cell with ITO electrodes and no alignment layer.

Table 3. Transition temperatures and associated entropy changes for **18-2-1** and **19-2-1**. The calculated dipole moments, μ , are also listed.

Compound	$T_{\text{ChI}}/^\circ\text{C}$	$T_{\text{NfI}}/^\circ\text{C}$	$\Delta S_{\text{ChI}}/R$	$\Delta S_{\text{NfI}}/R$	μ/D
18-2-1	133	^a 72	15.7	^a 1.27	12.69
19-2-1	154	^a 77	14.9	^a 1.32	13.78

^aValues extracted from DSC cooling traces.

T_{NI} of at least 180°C, and a $\text{N}_{\text{F}}\text{-I}$ transition is now seen at 104°C. The lowest value of the dipole moment for this group of molecules is seen for **11-0-1**, 10.33 D, those of **11-1-1** and **7-0-1** are rather similar, 11.36 D and 11.59 D, respectively, and **7-1-1** shows the highest value, 12.73 D. The decrease in T_{NI} on addition of a lateral methoxy group to **11-0-1** reflects the decreased structural anisotropy, see **Figure 10**, and the essentially identical values of T_{NI} shown by **7-0-1** and **11-1-1** imply that the effect on molecular shape of the substituents at these two different positions must be similar. Surprisingly, the fall in T_{NI} between **11-0-1** and **7-1-1** of at least 180°C is comparable to the sum of the decreases associated

with the addition of the two individual methoxy groups of 191°C indicating that in terms of shape, the first group does not, to any large extent, shield the second, **Figure 10**. It is striking that the addition of the lateral methoxy groups gives rise to the ferroelectric nematic phase. Attempts to measure a virtual value of $T_{\text{N}_{\text{F}}\text{N}}$ for the unsubstituted **11-0-1** using binary mixtures of **11-0-1** and **11-1-1** were not successful. These mixtures tended to phase separate and crystallise such that reliable data were not obtained and therefore a value of $T_{\text{N}_{\text{F}}\text{N}}$ for **11-0-1** could not be extrapolated. Although the addition of a methoxy group to the central phenyl ring in **11-1-1** (RM734) to give **7-1-1** reduces T_{NI} by at least 84°C, the

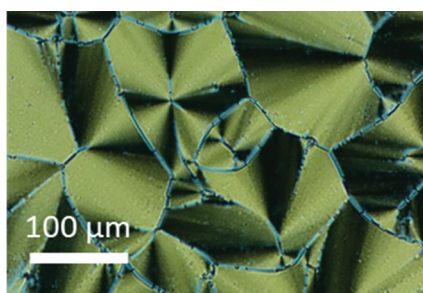


Figure 8. (Colour online) Polarised optical microscope texture observed for **19-2-1** in a cell treated for homeotropic alignment showing the banded texture of the N_F phase ($T = 74^\circ\text{C}$).

value of $T_{N_{FI}}$ seen for **7-1-1** is just 27°C lower than $T_{N_{FN}}$ for **11-1-1**. We will return to this issue later.

Extending the lateral methoxy group in **7-1-1** to ethoxy in **7-2-1** sees a drop in $T_{N_{FI}}$ of 23°C , whereas increasing the terminal group instead giving **7-1-2** is accompanied by a smaller reduction in $T_{N_{FI}}$ of 7°C . Making both changes to give **7-2-2** sees $T_{N_{FI}}$ fall by 25°C revealing that these effects are not simply additive. Increasing the length of the terminal substituent on the more biaxial molecule has a smaller relative effect such that $T_{N_{FI}}$ falls by just 2°C between **7-2-1** and **7-2-2** but by a larger amount between **7-1-2** and **7-2-2** of 18°C . It

should be noted that the dipole moments of these molecules are rather similar. Similar trends in $T_{N_{FI}}$ are observed for the corresponding fluorinated materials, the **8-*m-n*** series, although the magnitude of the differences between the corresponding members differ. This will be discussed in terms of the fluorine substituent later. It appears that the effects of increasing the terminal or lateral chain length on the relative stability of the N_F phase depends on how the shape of the molecule is changed, and that the N_F phase is favoured for a given shape or biaxiality either side of which it becomes less stable. The electrostatic potential surfaces of these materials show, **Figure 10**, that they all have regions of high and low electron density that alternate along the molecular long axis and are separated by the ester groups. It was suggested by Madhusudana [47], that such an arrangement stabilises the N_F phase.

This suggestion is supported by the behaviour of the **11-*m-n*** and **12-*m-n*** series, **Table 4**. These series contain a single lateral substituent, and increasing its length, *i.e.*, from **11-1-1** to **11-2-1** sees reductions in $T_{N_{FN}}$ and T_{NI} by 25°C and 57°C , respectively, whereas increasing the terminal chain length from **11-1-1** to **11-1-2** sees a much larger decrease in $T_{N_{FN}}$ of 45°C but a much smaller decrease in T_{NI} of just 6°C . The larger decrease in T_{NI}

Table 4. Transition temperatures and associated entropy changes for the **11-*m-n*** and **12-*m-n*** series. The calculated dipole moments, μ , are also listed.

<i>m</i>	<i>n</i>	X	$T_{Cr}/^\circ\text{C}$	$T_{N_{FI}}/^\circ\text{C}$ * $T_{N_{FI}}/^\circ\text{C}$	$T_{NI}/^\circ\text{C}$	$\Delta S_{Cr}/R$	$\Delta S_{N_{FI}}/R$ * $\Delta S_{N_{FI}}/R$	$\Delta S_{NI}/R$	μ/D	Ref
0	1	H	212	-	284	13.7	-	0.19	10.33	[22,46]
1	1	H	139	^a 131	188	9.96	^a 0.18	0.16	11.36	[10,12,25]
1	2	H	139	^a 86	182	10.2	^a 0.07	^a 0.16	^c 11.7	[10,45]
2	1	H	159	^a 106	^a 131	13.5	^a 0.14	^a 0.083	11.23	[18,40]
2	2	H	143	^a 91	^a 130	10.4	^a 0.07	^a 0.18	11.55	[10]
0	1	F	192	-	252	12.5	-	0.20	11.34	-
1	1	F	165	^a 140	^a 155	13.8	^a 0.47	0.14	12.39	[10]
1	2	F	142	^a 117	150	12.7	^a 0.12	0.085	^c 12.5	[10]
2	1	F	161	^a *109	-	11.9	^a *0.65	-	12.22	[40]
2	2	F	139	^b 105	^b 110	16.0	-	-	12.55	-

^aValues extracted from DSC cooling traces. ^bMeasured using polarised light microscopy. ^cLiterature value.

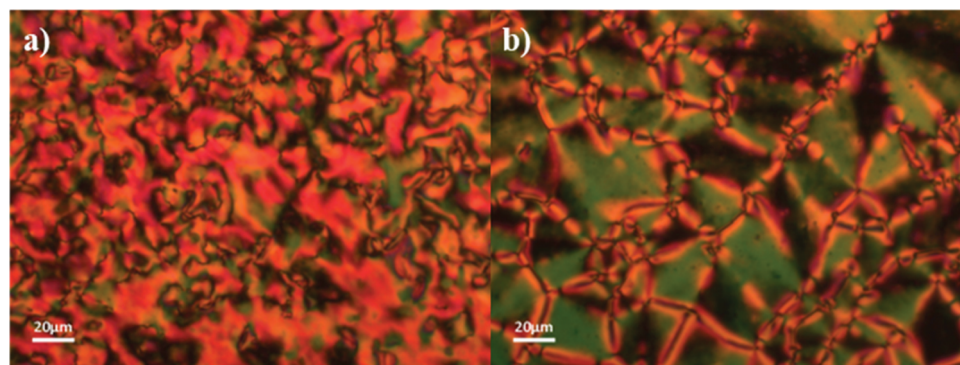


Figure 9. (Colour online) Polarised optical microscope textures observed for **12-2-2**: (a) schlieren texture of the N phase in untreated glass slides ($T = 108^\circ\text{C}$) and (b) banded texture of the N_F phase in a cell treated for planar alignment ($T = 102^\circ\text{C}$).

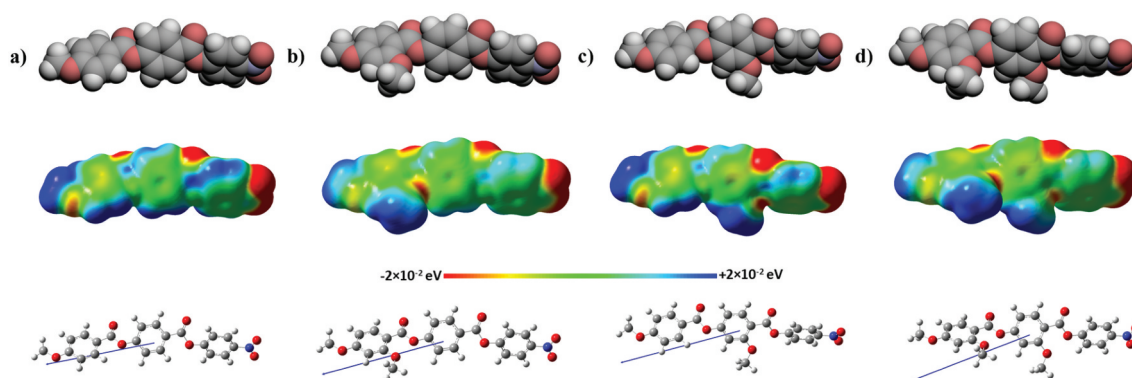


Figure 10. (Colour online) The space-filling models (top), electrostatic potential surfaces (middle) and ball-and-stick models of (a) **11-0-1**, (b) **11-1-1** (RM734), (c) **7-0-1** and (d) **7-1-1**, calculated at the B3LYP/6-31(d) level of theory. The arrow indicates the direction of the calculated dipole moment, with the head representing positive charge moving to the base which is negative.

on increasing the length of the lateral methoxy group in **11-1-1** reflects the reduction in shape anisotropy. By comparison, however, the increase in molecular biaxiality results in a smaller effect on $T_{N_{F,I}}$. The opposite behaviour is evident on increasing the length of the terminal methoxy group. On moving from **11-1-2** to **11-2-2**, the increase in the length of the lateral methoxy group reduces the shape anisotropy resulting in a large fall in T_{N_I} but increases $T_{N_{F,N}}$ suggesting that the increase in biaxiality is now more favourable to the formation of the N_F phase. As would be expected, the reverse is found moving from **11-2-1** to **11-2-2**, and increasing the length of the terminal chain has little effect on T_{N_I} but reduces $T_{N_{F,N}}$ by 15°C. Again, the trends in the transition temperatures of the corresponding fluorinated materials are the same although the magnitudes of the temperature differences change. The differences between the members of the **11- m - n** and **12- m - n** series on changing the values of m and n are larger than seen for the **7- m - n** and **8- m - n** series and this reflects the larger relative effect on molecular shape for the compounds containing a single lateral methoxy group.

Increasing the length of the methoxy group in the central ring in **7-1-1** to give **18-2-1**, Table 3, sees $T_{N_{F,I}}$ fall by 32°C compared to 23°C moving from **7-1-1** to **7-2-1**. Swapping the lateral groups in **7-2-1** to give **18-2-1** decreases $T_{N_{F,I}}$ by 9°C. Increasing the length of the chain has the greatest impact on $T_{N_{F,I}}$ if the chain is on the central ring although interchanging the ethoxy chain between the two rings has a much smaller effect. The extension of the methoxy to an ethoxy group clearly has a deleterious effect on the molecular shape but surprisingly, it is less important in which position the ethoxy group is in. This suggests that the optimum shape for the formation of the N_F phase is not necessarily a teardrop-like shape but rather depends on the

biaxiality of the molecule. Again, the trends are the same for the corresponding fluorinated compounds, **19-2-1**, **8-1-1** and **8-2-1**, although the differences between their values of $T_{N_{F,I}}$ are smaller. Presumably this reflects the smaller relative difference in shape arising from these structural changes given the effect of the lateral fluorine atom.

In Figure 11 we compare the transition temperatures of the materials containing lateral alkoxy groups on both the terminal and central phenyl rings, the **7- m - n** and **8- m - n** series, to those of the corresponding materials with only a single alkoxy group on either the terminal, the **11- m - n** and **12- m - n** series, or central phenyl ring, the **NT3- m** and **NT3F- m** series [36]. The addition of the second alkoxy group extinguishes the N phase but has a significantly weaker effect on the stability of the N_F phase. This reflects the greater sensitivity of the stability of the N phase to the reduction in shape anisotropy arising from the addition of the second lateral group. The stability of the N_F phase is also decreased by the addition of the second lateral group in each of the materials implying that the greater molecular biaxiality exceeds some optimum value as suggested earlier. The single exception to this observation is that the value of $T_{N_{F,I}}$ of **7-1-2** is 11°C higher than $T_{N_{F,N}}$ for **11-1-2**. The molecular dipole moment of the former is around 1.3 D greater. In our discussion so far, we have focussed on steric effects but as we will see electronic effects also play a significant role in determining the formation of the N_F phase and will return to this apparently anomalous observation later.

We now turn our attention to the effect of fluorine substitution on the stability of the N_F and N phases. The effects of adding a fluorine atom are twofold; specifically, the shape anisotropy of the molecules decreases, and the electronic properties of the molecule will change much more significantly than when extending a methoxy to an

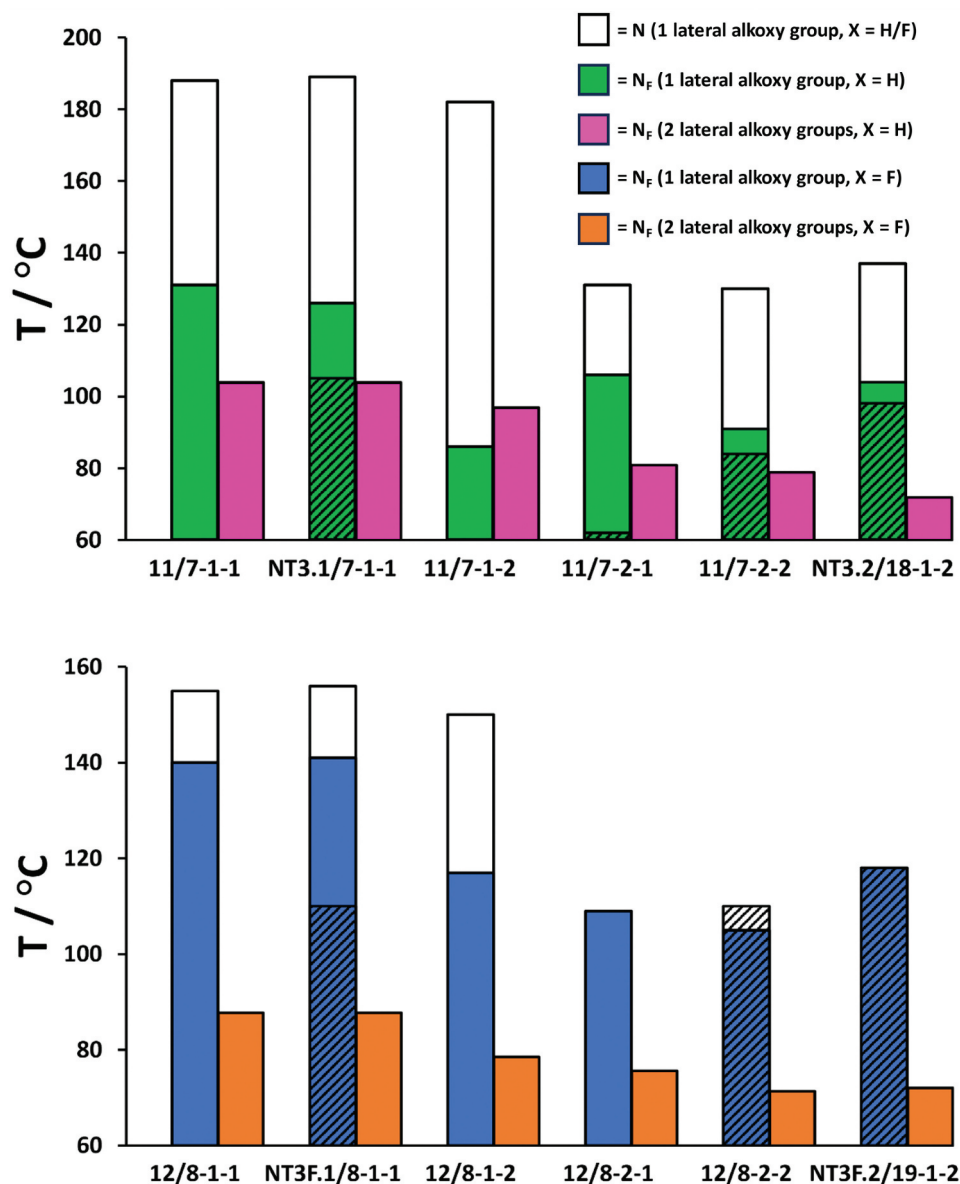


Figure 11. (Colour online) Comparison of the transition temperatures of the materials with a single alkoxy group (left bar) with the corresponding materials with two alkoxy groups (right bar). The top of the open bar shows the N-I transition and of the filled bar the N_F-N/I transition. Compounds with X = H (top) and with X = F (bottom). The shaded areas mark the temperature range in which the samples had crystallised on cooling as measured by DSC. The transition temperatures reported for **12-2-2** and **NT3F.2** were measured using polarised optical microscopy.

ethoxy group. Adding a fluorine atom to **11-0-1** to give **12-0-1** decreases T_{NI} by 32°C. The decrease between **7-0-1** and **8-0-1** in T_{NI} is also 32°C but this represents a greater relative change if expressed in terms of the ratio of the values of T_{NI} . This is a surprising observation given the addition of the fluorine atom may have been expected to have had a greater effect on the shape of the unsubstituted **11-0-1** than the methoxy substituted **7-0-1**. We do note, however, that the clearing temperature of **11-0-1** is very high such that partial decomposition may occur causing T_{NI} to be an underestimation. The fluorination of **7-0-1** to give **8-0-1** does increase $T_{N_{F,I}}$ by 16°C.

This structural change is associated with an increase in the dipole moment of around 1.0 D. **Figure 12** compares the values of $T_{N_{F,I}}$ for corresponding members of the *7-m-n* and *8-m-n* series, and of **18-2-1** and **19-2-1**. It is immediately apparent that there is no consistent effect over these five pairs of compounds. In three pairs, the addition of the fluorine atom increases $T_{N_{F,I}}$ and for two pairs we see a decrease. The increase in $T_{N_{F,I}}$ on addition of a fluorine atom *ortho* to the nitro group in this type of molecule has been interpreted within the framework of a molecular model that describes the formation of the N_F phase in which the molecules possess longitudinal surface

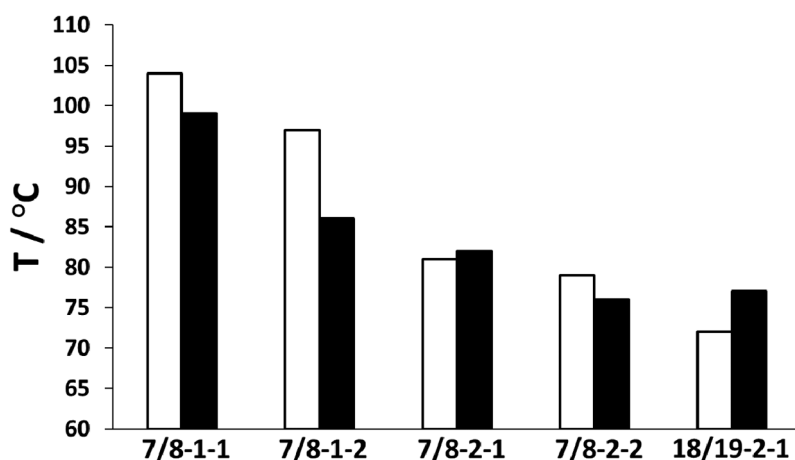


Figure 12. Comparison of the values of T_{NFI} of the **7-*m-n*** series (open bars) and **8-*m-n*** series (filled bars), with the top of the bars showing the transition to the N_F phase.

charge density waves and these interact inhibiting the formation of antiparallel structures [47]. The model reveals that parallel alignment is enhanced by reducing the amplitude of the charge density wave at either end of the molecule. The addition of the lateral fluorine substituent spreads electron density more evenly around the terminal ring as shown by the electrostatic potential surfaces, Figure 13, and this reduces the amplitude of the charge density wave which accounts for the increases in T_{NFI} observed. As we noted earlier, however, the addition of the fluorine atom also changes the shape of the molecule, Figure 13. We have seen that this may either promote or destabilise the N_F phase, and so

a competition exists between the steric and electronic effects. The two pairs of compounds in which T_{NFI} decreases on adding the fluorine atom both have lateral ethoxy groups and terminal methoxy groups. These compounds have the least anisometric shapes of this collection, and the addition of the fluorine atom presumably reduces this further leading to a greater decrease in the stability of the N_F phase which counteracts the positive electronic effect.

For the corresponding pairs of the **11-*m-n*** and **12-*m-n*** series, the addition of a fluorine atom *ortho* to the nitro group always decreases T_{NI} as would be expected based on the decrease in shape anisotropy and increases

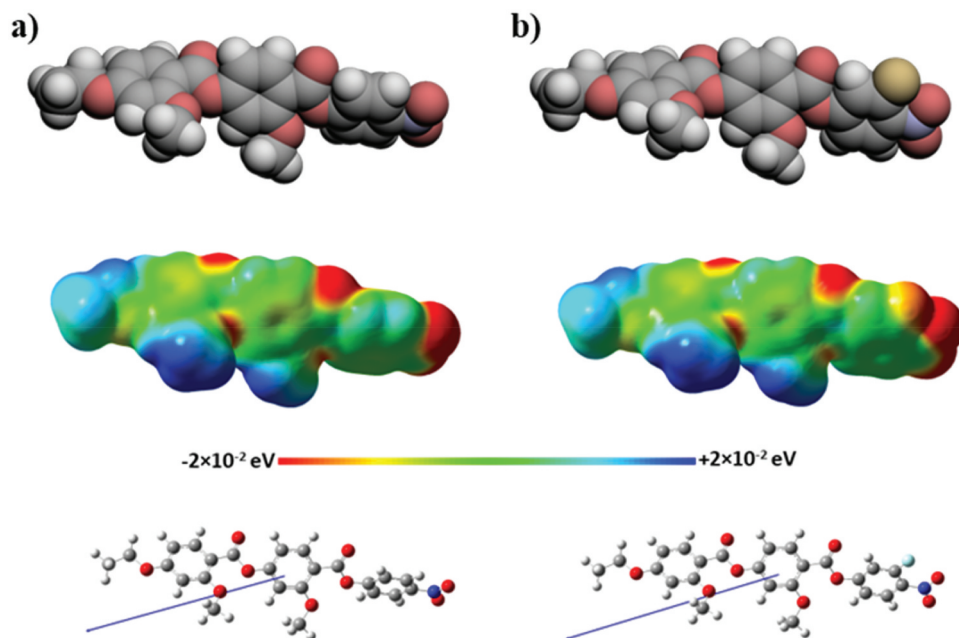


Figure 13. (Colour online) The space-filling models (top), electrostatic potential surfaces (middle) and ball-and-stick models of (a) **7-1-2**, and (b) **8-1-2**, calculated at the B3LYP/6-31(d) level of theory. The arrow indicates the direction of the calculated dipole moment, with the head representing positive charge moving to the base which is negative.

$T_{N_F N}$. Indeed, for **11-2-1** the addition of the fluorine atom sees the nematic phase extinguished and **12-2-1** shows a direct N_F -I transition. These series have just a single lateral methoxy or ethoxy group and so the effect on the molecular shape by the addition of a fluorine atom differs from that for the **7/8-*m-n*** and **18/19-2-1** materials. The largest difference in $T_{N_F N}$ is between **11-1-2** and **12-1-2** of 31°C, and the smallest is between **11-2-1** and **12-2-1** of just 3°C. This is consistent with our previous discussion such that **11-1-2** has the most anisometric shape of this collection and so the addition of a fluorine atom leads to the smallest overall change in biaxiality. As suggested earlier, this change in shape may promote the formation of the N_F phase complementing the electronic effect. By comparison, **11-2-1** has the least anisometric shape of this group and the addition of a fluorine atom presumably exacerbates this giving a shape that now destabilises the N_F phase. This counteracts the electronic effect of the fluorine atom leading to an overall smaller increase in $T_{N_F N}$.

We return now to the observation that value of $T_{N_F I}$ for **7-1-2** is 11°C higher than $T_{N_F N}$ for **11-1-2** and this was the only example for which a compound with two lateral groups shows a more stable N_F phase than the corresponding material with just a single lateral alkoxy group. The addition of a methoxy group to the central ring increases the charge density of this fragment which according to Madhusudana's model sees an increase in the stability of the N_F phase [47]. This will, of course, be true for each of these pairs of molecules but **11-1-2** has the most anisometric structure and so the addition of the methoxy group sees less of an increase in the molecular biaxiality. This combination of the electronic and shape considerations gives rise to the overall increase in the stability of the N_F phase. Finally, we commented earlier that the addition of a methoxy group to the central ring in **11-1-1** (RM734) to give **7-1-1** reduces T_{NI} by at least 84°C but the stability the N_F falls by just 27°C. These changes are consistent with the view that the electronic effect of adding the methoxy group to the central ring helps to offset the associated deleterious shape change and so the decrease in the stability of the N_F is less than may otherwise have been expected.

Conclusions

The relative stabilities of the N_F and N phases are governed by a subtle interplay of steric and electronic factors. The latter appear to be well described, at least qualitatively, within the framework of a molecular model developed by Madhusudana that describes the formation of the N_F phase in which the molecules possess longitudinal surface charge density waves and these interact inhibiting the

formation of antiparallel structures [47]. This approach is certainly more instructive than simply considering a molecular dipole moment. In addition to the electronic factors, it is clear that molecular shape plays a vital role in the formation of the N_F phase, and furthermore, to observe the N_F phase it appears that the molecular structure must include one or more lateral substituents that enhance molecular biaxiality and destabilise the N phase. From a molecular design viewpoint, the incorporation of lateral groups is a key factor in stabilising the N_F phase. There appears to be an optimum shape for the formation of the N_F phase and much work, both experimental and theoretical, is now required to understand this.

Disclosure statement

No potential conflict of interest was reported by the author(s).

Funding

C.T.I. and J.M.D.S. acknowledge the financial support of the Engineering and Physical Sciences Research Council [EP/V048775/1]. The research was also supported by the National Science Centre (Poland) under the grant no. [2021/43/B/ST5/00240].

ORCID

Ewan Cruickshank  <http://orcid.org/0000-0002-4670-8405>
 Naila Tufaha  <http://orcid.org/0000-0003-4042-7458>
 Rebecca Walker  <http://orcid.org/0000-0001-5167-7183>
 Stevie Brown  <http://orcid.org/0009-0004-7374-127X>
 Ewa Gorecka  <http://orcid.org/0000-0002-8076-5489>
 Damian Pociecha  <http://orcid.org/0000-0001-7734-3181>
 John M.D. Storey  <http://orcid.org/0000-0002-5261-5467>
 Corrie T. Imrie  <http://orcid.org/0000-0001-6497-5243>

References

- [1] Gray GW, Kelly SM. Liquid crystals for twisted nematic display devices. *J Mater Chem.* 1999;9(9):2037–2050. doi: 10.1039/a902682g
- [2] Chen HW, Lee JH, Lin BY, et al. Liquid crystal display and organic light-emitting diode display: present status and future perspectives. *Light Sci Appl.* 2017;7(3):17168–17168. doi: 10.1038/lsa.2017.168
- [3] Barnes, Anandan M, Lu D, et al. Wide color gamut LCD with a quantum dot backlight. *Opt Express.* 2013;21:26269–26284. doi:10.1364/OE.21.026269
- [4] Huang YM, Singh KJ, Liu AC, et al. Advances in quantum-dot-based displays. *Nanomaterials.* 2020;10(7):1327. doi: 10.3390/nano10071327
- [5] Mandle RJ. A new order of liquids: polar order in nematic liquid crystals. *Soft Matter.* 2022;18(27):5014–5020. doi: 10.1039/D2SM00543C

- [6] Sebastián N, Čopič M, Mertelj A. Ferroelectric nematic liquid-crystalline phases. *Phys Rev E*. 2022;106(2):021001. doi: [10.1103/PhysRevE.106.021001](https://doi.org/10.1103/PhysRevE.106.021001)
- [7] Born M. Über anisotrope Flüssigkeiten. Versuch einer Theorie der flüssigen Kristalle und des elektrischen Kerr-Effekts in Flüssigkeiten. *Sitzungsber Preuss Akad Wiss*. 1916;30:614–650.
- [8] Berardi R, Ricci M, Zannoni C. Ferroelectric nematic and smectic liquid crystals from tapered molecules. *Chemphyschem*. 2001;2(7):443–447. doi: [10.1002/1439-7641\(20010716\)2:7<443:AID-CPHC443>3.0.CO;2-J](https://doi.org/10.1002/1439-7641(20010716)2:7<443:AID-CPHC443>3.0.CO;2-J)
- [9] Berardi R, Ricci M, Zannoni C. Ferroelectric and structured phases from polar tapered mesogens. *Ferroelectrics*. 2004;309(1):3–13. doi: [10.1080/00150190490509674](https://doi.org/10.1080/00150190490509674)
- [10] Mandle RJ, Cowling SJ, Goodby JW. Rational design of rod-like liquid crystals exhibiting two nematic phases. *Chem A Eur J*. 2017;23(58):14554–14562. doi: [10.1002/chem.201702742](https://doi.org/10.1002/chem.201702742)
- [11] Nishikawa H, Shiroshita K, Higuchi H, et al. A fluid liquid-crystal material with highly polar order. *Adv Mater*. 2017;29(43):1702354. doi: [10.1002/adma.201702354](https://doi.org/10.1002/adma.201702354)
- [12] Chen X, Korblova E, Dong D, et al. First-principles experimental demonstration of ferroelectricity in a thermotropic nematic liquid crystal: polar domains and striking electro-optics. *Proc Natl Acad Sci*. 2020;117(25):14021–14031. doi: [10.1073/pnas.2002290117](https://doi.org/10.1073/pnas.2002290117)
- [13] Caimi F, Nava G, Barboza R, et al. Surface alignment of ferroelectric nematic liquid crystals. *Soft Matter*. 2021;17(35):8130–8139. doi: [10.1039/D1SM00734C](https://doi.org/10.1039/D1SM00734C)
- [14] Rudquist P. Revealing the polar nature of a ferroelectric nematic by means of circular alignment. *Sci Rep*. 2021;11(1):24411. doi: [10.1038/s41598-021-04028-7](https://doi.org/10.1038/s41598-021-04028-7)
- [15] Sebastián N, Cmok L, Mandle RJ, et al. Ferroelectric-ferroelastic phase transition in a nematic liquid crystal. *Phys Rev Lett*. 2020;124(3):037801. doi: [10.1103/PhysRevLett.124.037801](https://doi.org/10.1103/PhysRevLett.124.037801)
- [16] Folcia CL, Ortega J, Vidal R, et al. The ferroelectric nematic phase: an optimum liquid crystal candidate for nonlinear optics. *Liq Cryst*. 2022;49(6):899–906. doi: [10.1080/02678292.2022.2056927](https://doi.org/10.1080/02678292.2022.2056927)
- [17] Ortega J, Folcia CL, Etxebarria J, et al. Ferroelectric chiral nematic liquid crystals: new photonic materials with multiple bandgaps controllable by low electric fields. *Liq Cryst*. 2022;49(15):2128–2136. doi: [10.1080/02678292.2022.2104949](https://doi.org/10.1080/02678292.2022.2104949)
- [18] Pocięcha D, Walker R, Cruickshank E, et al. Intrinsically chiral ferronematic liquid crystals: an inversion of the helical twist sense at the chiral nematic – chiral ferronematic phase transition. *J Mol Liq*. 2021;361:119532. doi: [10.1016/j.molliq.2021.119532](https://doi.org/10.1016/j.molliq.2021.119532)
- [19] Zavvou E, Klasen-Memmer M, Manabe A, et al. Polarisation-driven magneto-optical and nonlinear-optical behaviour of a room-temperature ferroelectric nematic phase. *Soft Matter*. 2022;18(46):8804–8812. doi: [10.1039/D2SM01298G](https://doi.org/10.1039/D2SM01298G)
- [20] Nishikawa H, Sano K, Kurihara S, et al. Nano-clustering mediates phase transitions in a diastereomerically-stabilized ferroelectric nematic system. *Commun Mater*. 2022;3(1):89. doi: [10.1038/s43246-022-00312-9](https://doi.org/10.1038/s43246-022-00312-9)
- [21] Chen X, Korblova E, Glaser MA, et al. Polar in-plane surface orientation of a ferroelectric nematic liquid crystal: polar monodomains and twisted state electro-optics. *Proc Natl Acad Sci U S A*. 2021;118(22):e2104092118. doi: [10.1073/pnas.2104092118](https://doi.org/10.1073/pnas.2104092118)
- [22] Li J, Nishikawa H, Kougo J, et al. Development of ferroelectric nematic fluids with giant- ϵ dielectricity and nonlinear optical properties. *Sci Adv*. 2021;7(17):eabf5047. doi: [10.1126/sciadv.abf5047](https://doi.org/10.1126/sciadv.abf5047)
- [23] Li J, Wang Z, Deng M, et al. General phase-structure relationship in polar rod-shaped liquid crystals: importance of shape anisotropy and dipolar strength. *Giant*. 2022;11:100109. doi: [10.1016/j.giant.2022.100109](https://doi.org/10.1016/j.giant.2022.100109)
- [24] Saha R, Nepal P, Feng C, et al. Multiple ferroelectric nematic phases of a highly polar liquid crystal compound. *Liq Cryst*. 2022;49(13):1784–1796. doi: [10.1080/02678292.2022.2069297](https://doi.org/10.1080/02678292.2022.2069297)
- [25] Brown S, Cruickshank E, Storey JMD, et al. Multiple polar and non-polar nematic phases. *Chemphyschem*. 2021;22(24):2506–2510. doi: [10.1002/cphc.202100644](https://doi.org/10.1002/cphc.202100644)
- [26] Nishikawa H, Sano K, Araoka F. Anisotropic fluid with phototunable dielectric permittivity. *Nat Commun*. 2022;13(1):1142. doi: [10.1038/s41467-022-28763-1](https://doi.org/10.1038/s41467-022-28763-1)
- [27] Mandle RJ, Sebastián N, Martínez-Perdiguero J, et al. On the molecular origins of the ferroelectric splay nematic phase. *Nat Commun*. 2021;12(1):4962. doi: [10.1038/s41467-021-25231-0](https://doi.org/10.1038/s41467-021-25231-0)
- [28] Manabe A, Bremer M, Kraska M. Ferroelectric nematic phase at and below room temperature. *Liq Cryst*. 2021;48(8):1079–1086. doi: [10.1080/02678292.2021.1921867](https://doi.org/10.1080/02678292.2021.1921867)
- [29] Li J, Xia R, Xu H, et al. How far can we push the rigid oligomers/polymers toward ferroelectric nematic liquid crystals? *J Am Chem Soc*. 2021;143(42):17857–17861. doi: [10.1021/jacs.1c09594](https://doi.org/10.1021/jacs.1c09594)
- [30] Vaupotič N, Pocięcha D, Rybak P, et al. Dielectric response of a ferroelectric nematic liquid crystalline phase in thin cells. *Liq Cryst*. 2023;50(4):584–595. doi: [10.1080/02678292.2023.2180099](https://doi.org/10.1080/02678292.2023.2180099)
- [31] Nishikawa H, Araoka F. A new class of chiral nematic phase with helical polar order. *Adv Mater*. 2021;33(35):2101305. doi: [10.1002/adma.202101305](https://doi.org/10.1002/adma.202101305)
- [32] Chen X, Zhu Z, Magrini MJ, et al. Ideal mixing of paraelectric and ferroelectric nematic phases in liquid crystals of distinct molecular species. *Liq Cryst*. 2022;49(11):1531–1544. doi: [10.1080/02678292.2022.2058101](https://doi.org/10.1080/02678292.2022.2058101)
- [33] Sebastián N, Mandle RJ, Petelin A, et al. Electrooptics of mm-scale polar domains in the ferroelectric nematic phase. *Liq Cryst*. 2021;48(14):2055–2071. doi: [10.1080/02678292.2021.1955417](https://doi.org/10.1080/02678292.2021.1955417)
- [34] Song Y, Deng M, Wang Z, et al. Emerging ferroelectric uniaxial lamellar (smectic AF) fluids for bistable In-plane polarization memory. *J Phys Chem Lett*. 2022;13(42):9983–9990. doi: [10.1021/acs.jpcllett.2c02846](https://doi.org/10.1021/acs.jpcllett.2c02846)
- [35] Feng C, Walba D, Korblova E, et al. Electrically tunable reflection color of chiral ferroelectric nematic liquid crystals. *Adv Opt Mater*. 2021;9(22):2101230. doi: [10.1002/adom.202101230](https://doi.org/10.1002/adom.202101230)
- [36] Tufaha N, Cruickshank E, Pocięcha D, et al. Molecular shape, electronic factors and the ferroelectric nematic

- phase. *Chem A Eur J.* **2023**;29(28):e202300073. doi: [10.1002/chem.202300073](https://doi.org/10.1002/chem.202300073)
- [37] Kikuchi H, Matsukizono H, Iwamatsu K, et al. Fluid layered ferroelectrics with global $C_{\infty v}$ symmetry. *Adv Sci.* **2022**;9(26):2202048. doi: [10.1002/advs.202202048](https://doi.org/10.1002/advs.202202048)
- [38] Matsukizono H, Iwamatsu K, Endo S, et al. Synthesis of liquid crystals bearing 1,3-dioxane structures and characterization of their ferroelectricity in the nematic phase. *J Mater Chem C.* **2023**;11(18):6183–6190. doi: [10.1039/D2TC05363B](https://doi.org/10.1039/D2TC05363B)
- [39] Cruickshank E, Pearson A, Brown S, et al. The ferroelectric nematic phase: on the role of lateral alkyloxy chains. *Liq Cryst.* **2023**;50(11):1960–1967. doi: [10.1080/02678292.2023.2221651](https://doi.org/10.1080/02678292.2023.2221651)
- [40] Cruickshank E, Walker R, Storey JMD, et al. The effect of a lateral alkyloxy chain on the ferroelectric nematic phase. *RSC Adv.* **2022**;12(45):29482–29490. doi: [10.1039/D2RA05628C](https://doi.org/10.1039/D2RA05628C)
- [41] Mandle RJ. Automated flow synthesis of algorithmically designed ferroelectric nematogens. *Liq Cryst.* **2023**;50(3):534–542. doi: [10.1080/02678292.2023.2208550](https://doi.org/10.1080/02678292.2023.2208550)
- [42] Frisch MJ, Trucks GW, Schlegel HB, et al. Gaussian 09, revision B.01. Gaussian 09, revision B.01. Wallingford CT, Gaussian, Inc; (2010).
- [43] Tarini M, Cignoni P, Montani C. Ambient occlusion and edge cueing to enhance real time molecular visualization. *IEEE Trans Vis Comput Graph.* **2006**;12(5):1237–1244. doi: [10.1109/TVCG.2006.115](https://doi.org/10.1109/TVCG.2006.115)
- [44] Perera K, Saha R, Nepal P, et al. Ferroelectric nematic droplets in their isotropic melt. *Soft Matter.* **2023**;19(3):347–354. doi: [10.1039/D2SM01395A](https://doi.org/10.1039/D2SM01395A)
- [45] Mandle RJ, Cowling SJ, Goodby JW. Structural variants of RM734 in the design of splay nematic materials. *Liq Cryst.* **2021**;48(12):1780–1790. doi: [10.1080/02678292.2021.1934740](https://doi.org/10.1080/02678292.2021.1934740)
- [46] Mandle RJ, Cowling SJ, Goodby JW. A nematic to nematic transformation exhibited by a rod-like liquid crystal. *Phys Chem Chem Phys.* **2017**;19(18):11429–11435. doi: [10.1039/C7CP00456G](https://doi.org/10.1039/C7CP00456G)
- [47] Madhusudana NV. Simple molecular model for ferroelectric nematic liquid crystals exhibited by small rod-like mesogens. *Phys Rev E.* **2021**;104(1):014704. doi: [10.1103/PhysRevE.104.014704](https://doi.org/10.1103/PhysRevE.104.014704)